International Journal of Automotive Technology, Vol. 18, No. 3, pp. 499–504 (2017)
DOI 10.1007/s12239–017–0049–x

pISSN 1229–9138/ eISSN 1976–3832

DESIGN OF FERRITE MAGNET CFSM TO IMPROVE SPEED RESPONSE OF EPS SYSTEM

Myung-Seop Lim, Dong-Min Kim and Jung-Pyo Hong*

Automotive Engineering, Hangyang University, Seoul 04763, Korea

(Received 3 March 2016; Revised 9 November 2016; Accepted 16 November 2016)

ABSTRACT–This paper deals with the speed response characteristic of the concentrated flux synchronous motor (CFSM) using ferrite magnets for the electric power steering (EPS) system. To analyze the response characteristic of the CFSM, an analytical method using the electromechanical undamped natural frequency and damping ratio based on the transfer function is proposed. By using the method, the speed response according to the variations of the shape of the permanent magnets (PMs) and rotor core is analyzed. It was analyzed under the conditions of the constant volume of the PMs as well as the constant diameter of the rotor. By using the proposed analysis method, the improved model is desgined based on the initial model fulfilling the required specifications. Finally, the torque and speed response characteristics of two motors are simulated through the finite element analysis (FEA) and MATLAB Simulink.

KEY WORDS : Concentrated Flux Synchronous Motor (CFSM), Damping ratio, Electric Power Steering (EPS), Electromechanical undamped natural frequency, Ferrite magnet, Speed response characteristic, Mass moment of inertia

1. INTRODUCTION

Environmental regulations and large demands on convenience for drivers accelerate electrification in the vehicle industry. As electrification of vehicles has been progressed, the hydraulic power steering (HPS) systems replaced by the electric power steering (EPS) systems. EPS offers several advantages over conventional HPS, such as improved fuel economy and elimination of hydraulic fluid (Lee *et al*., 2014; Jang *et al*., 2015). As a motor for EPS, the permanent magnet synchronous motor (PMSM) has been adopted due to its high power density and efficiency. Particularly, a rare-earth-free synchronous motor such as ferrite magnet concentrated flux synchronous motors (CFSMs) is developed as the EPS motors because the price instability of the rare-earth permanent magnets (PMs). However, the power density of the ferrite magnet CFSMs is relatively smaller than those of the rare-earth PMSMs. Therefore, the diameter of the rotor and stator should be increased to achieve the same performance of the rare-earth PMSMs. However, the size of the PM and rotor configuration have a significantly affect on the speed response of the EPS system. The speed response characteristic of the EPS motors affects the steering safety and drivability of the drivers. Thus, it is necessary to investigate the speed response characteristic of the ferrite magnet EPS motor.

There are some prior works about the system response or control methods of the EPS system from the view point of the controller designers (Chen *et al*., 2008; Wang *et al*., 2009; Shriwastava and Diagavane, 2011; Lee *et al*., 2011, 2012). Some previous papers only discuss the design method of the EPS motor to reduce cogging torque or torque ripple even though the speed response characteristics are very important in the EPS system (Kim *et al*., 2014; Saha *et al*., 2015; Kim *et al*., 2010; Ombach and Junak, 2007). However, there are few prior researches on the design methods of the EPS motor to achieve fast speed response from the view point of the electric machine designer. Hence, this paper deals with the analytical method to design the ferrite magnet CFSM to achieve the fast speed response. At first, the analytic methods to find the CFSM parameters are presented. Secondly, the method to analyze the speed response characteristic of the motor based on the mathematical model is proposed. Thirdly, based on the analysis results obtained by using the proposed method, the shape of the PM and rotor configuration of the initial model are changed to propose the improved model. For the improved design, the rotor outer diameter and the volume of the each PM is maintained. Finally, the torque performances and the speed response characteristics of the initial model and improved model are presented and compared by using finite element analysis (FEA) and Matlab Simulink.

2. CALCULATION OF MOTOR PARAMETERS

The motor parameters which are needed to investigate the

**Corresponding author.* e-mail: hongjp@hanyang.ac.kr

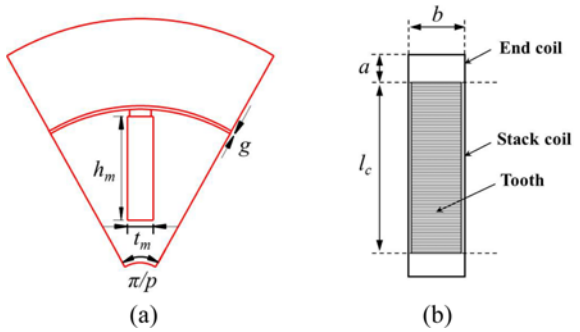

Figure 1. Geometry define of the CFSM used in the analytical approach: (a) Front view of the CFSM for one pole; (b) Top vew of the stator tooth and coil.

Table 1. Densities of materials used in the motor.

Items	Magnet	Core	Shaft
Density (kg/m^3)	5000	7850	2712

speed response characteristic were obtained by the analytical approaches. Therefore, the mathematical models to find the parameters are organized in this paper. The parameters are phase resistance, inductance, back electromotive force (BEMF), and mass moment of inertia of the rotor. The geometry of the 14 pole-18 slot CFSM used in this study is shown in Figure 1.

2.1. Resistance

The phase resistance in the armature is dependent on the length of the coil, the cross-sectional area of the conductor, and the operating temperature. The 14 pole-18 slot CFSM has the concentrated winding in the stator, and the space factor of the slot is 43 %. The operating temperature of the coil in the EPS motor is assumed as 60 °C.

$$R_a = \frac{l_{coil}}{\sigma S_{copper}} = \frac{(4a+2b+2l_c)N}{\sigma S_{copper}} \tag{1}$$

where l_{coil} is the length of the coil, and σ is the conductivity of the conductor. S_{copper} is cross-sectional area of the conductor, and N is the coil turn number.

2.2. Inductance

The d, q-axis inductances are calculated by considering the PM shape as well as the configuration of the rotor (Hendershot and Miller, 2010). Slot leakage and harmonic inductances are neglected. d-axis inductance L_d is

$$L_d = \frac{3}{\pi}\frac{\mu_0 D L_{stk}}{g}\left(\frac{k_w N}{P_n}\right)^2\left(1-\frac{\frac{4}{\pi}}{\frac{\pi}{2}+4P_n\frac{g\mu_r}{t_m}\frac{h_m}{D}}\right) \tag{2}$$

and, q-axis inductance L_q is

$$L_q = \frac{3}{\pi}\frac{\mu_0 D L_{stk}}{g}\left(\frac{k_w N}{P_n}\right)^2 \tag{3}$$

where μ_0 and μ_r are the permeability of free space and the relative permeability of core in H/m, respectively. D is the rotor outer diameter in mm. L_{stk} is the stack length of the stator, and g is the air-gap length. k_w is the winding factor, and P_n is the number of pole-pair. t_m and h_m are the thickness and height of the PM in mm, respectively.

2.3. Back Electromotive Force

The air-gap flux density B_{gm} is obtained through the Gauss' law and Ampere's law. Equation (4) is derived as the result. In this process, the saturation of the core and irreversible demagnetization of the PM are not considered.

$$B_{gm} = \frac{B_{rem}}{\frac{\pi D}{4ph_m}+\frac{2\mu_{rec}g}{t_m}} \tag{4}$$

where B_{rem} is the residual induction in T. p and μ_{rec} are pole number and the recoil permeability of PM, respectively.

Based on (4), the BEMF E_a of the CFSM is calculated by considering the winding factor, turn number, stack length, and geometric dimensions. The derived equation is shown in (5).

$$E_a = \omega\Psi_m = \omega\frac{4}{\pi}\frac{k_w N}{2}\frac{DL_{stk}}{p}B_{gm} \tag{5}$$

where ω is the electrical angular speed in rad/s, and Ψ_m is the linkage flux in Wb.

2.4. Mass Moment of Inertia

For the CFSM in this study, electrical steel S60 is used as the core material, and NMF-12G ferrite magnet is used. For the shaft material, aluminum, non-magnetic material, is used to avoid leakage of flux. The densities of the materials are organized in Table 1. The mass moment of inertia of the rotor J can be calculated from the definition of the mass moment of inertia and the parallel-axis theorem.

$$J = J_{core} + J_{PM}$$

$$\begin{cases} J_{core} = \int_{m_{core}} r_i^2 dm_i \\ J_{PM} = p\cdot\left(\int_{m_{PM}} r_j^2 dm_j + m_{PM}d^2\right) \end{cases} \tag{6}$$

where $m_{i,j}$ is the mass of each small particles in the rotor core and PM. $r_{i,j}$ is the distance between each small particles and the center of mass in the rotor core and PM. m_{core} and m_{PM} are the entire mass of the rotor core and PM, respectively. d is the distance between the center of PM mass and the center of rotation.

3. SPEED RESPONSE CHARACTERISTIC

The proposed method to analyze the speed response

characteristic is based on the mathematical model of an electric motor. For the method, the transfer function of the machine was deduced, and the two objective functions representing for the speed response characteristic were derived. Finally, the values of the design parameters were determined based on the derived objective functions.

3.1. Motor Model in Laplace Domain

To analyze the speed response characteristic of electric motors, a mathematical model was used. The motors can be expressed simply by using both electrical and mechanical equations. They are voltage equation and torque equation, respectively. The voltage equation of the electric motor is

$$\begin{aligned} V_{\mathrm{a}} &= R_{\mathrm{a}} i_{\mathrm{a}} + L_{\mathrm{a}} \frac{di_{\mathrm{a}}}{dt} + E_{\mathrm{a}} \\ &= R_{\mathrm{a}} i_{\mathrm{a}} + L_{\mathrm{a}} \frac{di_{\mathrm{a}}}{dt} + k_{\mathrm{E}} \phi_{\mathrm{f}} \omega_{\mathrm{m}} \end{aligned} \tag{7}$$

where V_{a} and i_{a} are the armature voltage and current; R_{a} and L_{a} are the armature coil resistance and the phase inductance; L_a is the average value of the L_{d} and L_{q} obtained from (2) and (3). E_{a} is BEMF in rms. k_{E} and ϕ_{f} are the BEMF constant and field flux. ω_{m} is the mechanical speeds in rad/s. The torque equation is

$$\begin{aligned} T_{\mathrm{e}} &= J \frac{d\omega_{\mathrm{m}}}{dt} + B\omega_{\mathrm{m}} + T_{\mathrm{L}} \\ &= k_{\mathrm{T}} \phi_{\mathrm{f}} i_{\mathrm{a}} \end{aligned} \tag{8}$$

where J and B are the mass moment of inertia and friction coefficient; T_{e} and k_{t} are the electric torque and torque constant. ω_{m} and T_{L} are the mechanical speeds in rad/s and load torque. In this study, it was assumed that load torque T_{L} is zero, and it can be neglected in the follow equations.

Laplace transformation of (7) and (8) was conducted to find the transfer function of the machine in Laplace domain. As the results, the voltage equation is

$$\begin{aligned} V_{\mathrm{a}}(s) &= (R_{\mathrm{a}} + sL_{\mathrm{a}}) i_{\mathrm{a}}(s) + E_{\mathrm{a}}(s) \\ &= (R_{\mathrm{a}} + sL_{\mathrm{a}}) i_{\mathrm{a}}(s) + k_{\mathrm{E}} \phi_{\mathrm{f}} \omega_{\mathrm{m}}(s) \end{aligned} \tag{9}$$

and the torque equation is

$$\begin{aligned} T_{\mathrm{e}}(s) &= (sJ + B) \omega_{\mathrm{m}}(s) \\ &= k_{\mathrm{T}} \phi_{\mathrm{f}} i_{\mathrm{a}}(s) \end{aligned} \tag{10}$$

Based on the (9) and (10), a block diagram and transfer function can be deducted.

3.2. Transfer Function

The block diagram of an electric motor is shown in Figure 2. From the diagram, the transfer function in Laplace domain can be obtained.

$$\frac{\omega_{\mathrm{m}}}{V_{\mathrm{a}}} = \frac{\frac{1}{sL_{\mathrm{a}} + R_{\mathrm{a}}} \cdot k_{\mathrm{T}} \phi_{\mathrm{f}} \cdot \frac{1}{sJ + B}}{1 + \left(\frac{1}{sL_{\mathrm{a}} + R_{\mathrm{a}}} \cdot k_{\mathrm{T}} \phi_{\mathrm{f}} \cdot \frac{1}{sJ + B} \right) \cdot k_{\mathrm{E}} \phi_{\mathrm{f}}} \tag{11}$$

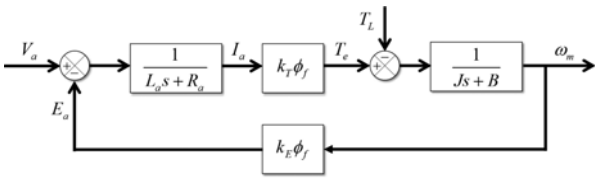

Figure 2. Block diagram of the electric motor transfer function.

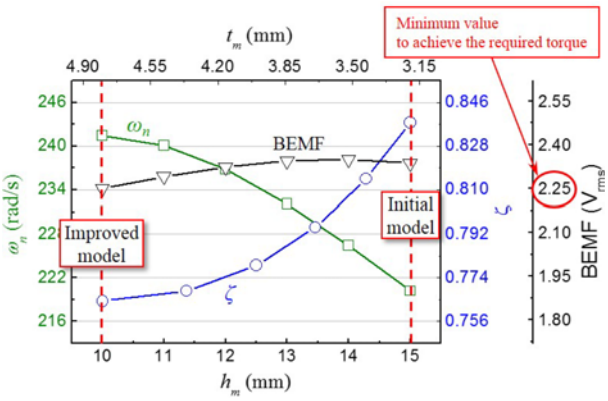

Figure 3. Tendency of the speed response characteristics according to the PM shapes in the CFSM.

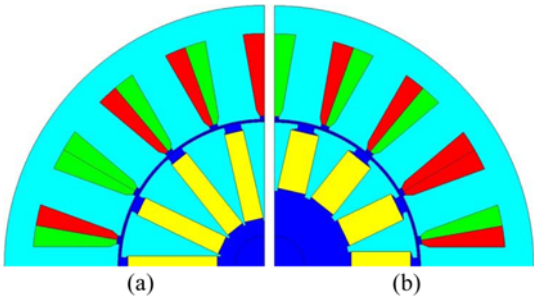

Figure 4. Proposed models: (a) Initial model; (b) Improved model.

Equation (11) can be organized by 2nd order standard form as below.

$$\frac{\omega_{\mathrm{m}}}{V_{\mathrm{a}}} = \frac{\frac{K}{JL_{\mathrm{a}}}}{s^2 + \left(\frac{R_{\mathrm{a}}}{L_{\mathrm{a}}} + \frac{B}{J} \right) s + \left(\frac{R_{\mathrm{a}}}{L_{\mathrm{a}}} \cdot \frac{B}{J} + \frac{K^2}{JL_{\mathrm{a}}} \right)} \tag{12}$$

where

$$k_{\mathrm{E}} \phi_{\mathrm{f}} = k_{\mathrm{T}} \phi_{\mathrm{f}} = K \tag{13}$$

From (12), the electromechanical undamped natural frequency ω_{n} and damping ratio ζ can be obtained as (14) and (15).

$$\omega_{\mathrm{n}} = \sqrt{\frac{B}{J} \cdot \frac{R_{\mathrm{a}}}{L_{\mathrm{a}}} + \frac{K^2}{JL_{\mathrm{a}}}} \tag{14}$$

Table 2. Densities of materials used in the motor.

Items	Initial model	Improved model
Pole / Slot	14 / 18	
L_{stk} (mm)	39	
D (mm)	48	
h_m (mm)	15	10
t_m (mm)	3.2	4.8
R_a (mΩ)	16.6	
L_a (mH)	0.045	0.041
J (kg·m^2)	1.686×10^{-3}	1.512×10^{-3}
B (kg·m^2/s)	1.0×10^{-4}	
ω_n (rad/s)	241.4	316.7
ζ	0.77	0.64

$$\zeta = \frac{\frac{B}{J} + \frac{R_a}{L_a}}{2\sqrt{\frac{B}{J} \cdot \frac{R_a}{L_a} + \frac{K^2}{JL_a}}} \tag{15}$$

The high electromechanical undamped natural frequency ω_n and low damping ratio ζ can lead to the fast response speed of the electric machines (Dorf and Bishop, 2010). Therefore, in this study, ω_n and ζ were used as the objective functions to estimate the speed response characteristic of the EPS motors.

4. COMPARISON OF INITIAL AND IMPROVED MODES

In this study, two CFSMs which has different rotor shape are proposed. They are the initial model and the improved model. The initial model is determined to fulfill the required specifications. The thickness t_m and height h_m of the PMs are 3.2 mm and 15 mm, respectively. Based on the initial model, the improved model is designed through the proposed analysis method to achieve the fast speed response. The tendency of the speed response characteristics such as the ω_n and ζ as well as magnitude of the BEMF according to the variations of the PMs shapes is presented in Figure 3. t_m and h_m should not need to be integers, theoretically, because they are variables about the dimensions of a PM. Therefore, there is an infinite number of combinations of t_m and h_m. Consequently, the numbers of ω_n and ζ is no limited, theoretically. They were analyzed under the conditions of the constant volume of the PMs as well as the constant diameter of the rotor. Given the ω_n and ζ of the analysis results, increasing thickness t_m and decreasing height h_m of the PMs make improvement of the speed response of the CFSM. However, given the magnitude of the BEMF in Figure 3, further decrease in h_m under 10 mm and increase in t_m of 4.8 mm cause that the designed machine cannot fulfill the required torque and power. This is due to the fact that the magnitude of the BEMF should be 2.25 V_{rms} at least to achieve the required torque and power considering the input current limitation. Therefore, the t_m and h_m for the improved model were determined as 4.8 mm and 10 mm, respectively. The configurations and parameters of the motors are shown in Figure 4 and Table 2. Lastly, by using the FEA and Matlab Simulink, the torque performance and speed response are simulated and compared to verify the validity of the proposed analysis method.

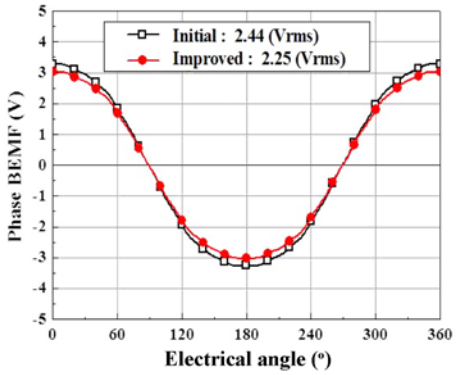

Figure 5. BEMF of the proposed models.

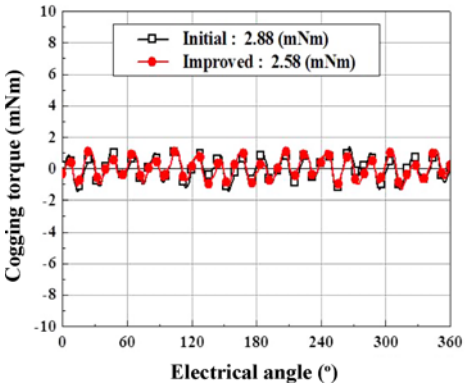

Figure 6. Cogging torque of the proposed models.

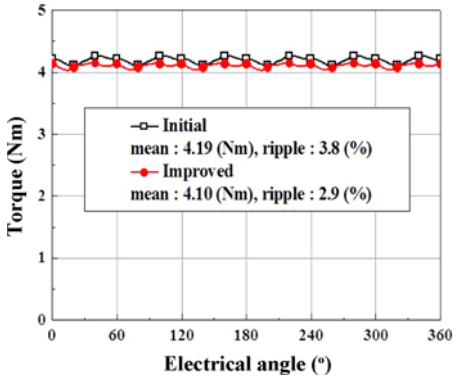

Figure 7. Torque ripple of the proposed models.

Table 3. Load conditions and FEA results of models.

Items	Initial model	Improved model
DC link voltage (V)	12	
Current limit (A_{rms})	60	
Phase BEMF (V)	2.44	2.25
Torque (Nm)	4.19	4.10
Torque ripple (%)	3.8	2.9
Cogging torque (mNm)	2.88	2.58

4.1. Performance

BEMF at 1,000 rpm and cogging torque of the proposed motors under no-load condition are shown in Figure 5 and Figure 6. Also, Figure 7 presents the torque ripple of the motors under the 60 A_{rms} load condition. Given the results, the BEMF and cogging torque are decreased about 7.8 % and 10.4 %, respectively. The torque ripple is reduced by 0.9 %. Thus, it can be concluded that the torque characteristics of the improved model are excellent rather than those of the initial model. All of the results are obtained via the nonlinear FEA. The load conditions and nonlinear FEA results are organized in Table 3.

4.2. Speed Response

Apart from the torque performance, the rise time is analyzed to compare the speed response characteristics of the motors. The analysis results are obtained by using the Matlab Simulink. Figures 8 and 9 present the response characteristic to the unit step input without and with PI controller, respectively. Figure 10 shows the speed response of the machines with PI controller considering the actual voltage and current limitations. Assuming that there are no limitations of the current and voltage of the controllers, fast rise time can be achieved since the high voltage and current can be applied to the machines in an instant. However, there are limitations of the voltage and current for the actual controllers. Therefore, speed response and rise time

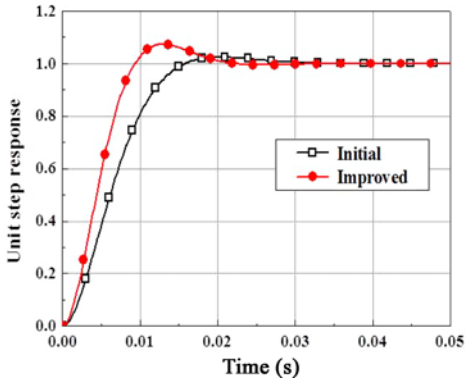

Figure 8. Speed response of each model.

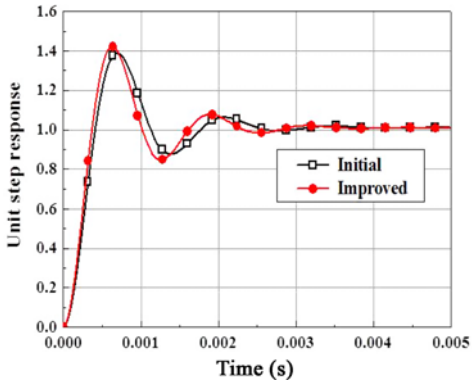

Figure 9. Speed reponse of each model with controller.

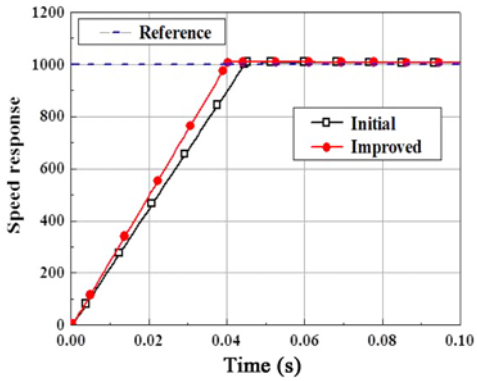

Figure 10. Speed reponse of each model with controller considering the actual voltage and current limitations.

Table 4. Speed response characteristics of each model.

Items		Initial model	Improved model
Rise time (msec)	Motor	11.9	7.8
	Motor with PI controller	1.54	0.32
	Motor with PI controller considering limitations	40.2	36.1

of the machines considering the actual voltage and current limitations of the controllers are belated and delayed comparing to those of the unlimited voltage and current conditions of the controllers. Consequently, 'limitations' means that the maximum input voltage and current that the controller can apply to the electric machine. Given the results, the rise time decreased by 4.10 msec, 1.22 msec, and 4.10 msec according to the simulation conditions. The rise times of the motors are organized in Table 4. Consequently, it is verified that the speed responses of the machine can be improved due to the proposed method.

5. CONCLUSION

The analytical method to improve the speed response of the CFSM by redesigning the shape of the rotor was presented in this study. Based on the proposed method, the improved motor fulfilling both the required specifications and fast speed response was proposed. The BEMF of the improved motor was decreased by 7.8 %, but the cogging torque and torque ripple of the improved motor was decreased by 10.4 % and 0.9 %, respectively, comparing to those of the initial motor. Also, the rise time was reduced about 10.2 % ~ 79.2 %. Consequently, the proposed analytical method was useful to design the CFSM to achieve the fast speed response.

ACKNOWLEDGEMENT–This research was supported by the MSIP (Ministry of Science, ICT and Future Planning), Korea, under the ITRC (Information Technology Research Center) (IITP-2016-H8601-16-1005) supervised by the IITP (Institute for Information & Communication Technology Promotion).

REFERENCES

Chen, X., Yang, T., Chen, X. and Zhou, K. (2008). A generic model-based advanced control of electric power-assisted steering systems. *IEEE Trans. Control Systems Technology* **16**, **6**, 1289–1300.

Dorf, R. C. and Bishop, R. H. (2010). *Modern Control Systems*. 12th edn. Prentice Hall. New Jersey, USA.

Hendershot, J. R. and Miller, T. J. E. (2010). *Design of Brushless Permanent Magnet Machine*. 2nd edn. Motor Design Books LLC. Florida, USA.

Jang, J. Y., Cho, S. G., Lee, S. J., Kim, K. S., Kim, J. M., Hong, J. P. and Lee, T. H. (2015). Reliability-based robust design optimization with kernal density estimation for electric power steering motor considering manufacturing uncertainties. *IEEE Trans. Magnetics* **51**, **3**, 8001904.

Kim, Y. B., Kim, H. J., Jung, K. T. and Hong, J. P. (2014). Influence of manufacturing tolerances on cogging torque of IPMSM for EPS application. *IEEE Int. Conf. Electric Machines and Systems*, 382–386.

Kim, Y. K., Rhyu, S. H. and Jung, I. S. (2010). Shape optimization for reduction the cogging torque of BLAC motor for EPS application. *IEEE Int. Conf. Electric Machines and Systems*, 1163–1167.

Lee, G. H., Choi, W. C., Kim, S. I., Kwon, S. O. and Hong, J. P. (2011). Torque ripple minimization control of permanent magnet synchronous motors for EPS applications. *Int. J. Automotive Technology* **12**, **2**, 291–297.

Lee, J. H., Moon, H. T. and Yoo, J. Y. (2012). Current sensorelss drive method for electric power steering. *Int. J. Automotive Technology* **13**, **7**, 1141–1147.

Lee, S. J., Kim, S. I. and Hong, J. P. (2014). Characteristics of PM synchronous motors according to pole-slot combinations for EPS applications. *Int. J. Automotive Technology* **15**, **7**, 1183–1187.

Ombach, G. and Junak, J. (2007). Two rotors design's comparison of permanent magnet brushless synchronous motor for and electric power steering application. *European Conf. Power Electronics and Applications*, 1–9.

Saha, S., Kim, S. A. and Cho, Y. H. (2015). Optimal rotor shape design for minimizing cogging torque of spoke type BLAC motor for EPS. *IEEE Int. Conf. Industrial Electronics and Applications*, 1313–1318.

Shriwastava, R. G. and Diagavane, M. B. (2011). Electric power steering with permanent magnet synchronous motor drive used in automotive application. *Int. Conf. Electrical Energy Systems*, 145–148.

Wang, S., Yin, C. and Zhao, J. (2009). Design and full-vehicle tests of EPS control system. *Int. Forum on Computer Science-Technology and Applications*, 101–104.